SLAC–PUB–7826
June 1998

A preliminary improved measurement of the B hadron energy distribution in Z^0 decays *

The SLD Collaboration**
Stanford Linear Accelerator Center
Stanford University, Stanford, CA 94309

ABSTRACT

We have measured the B hadron energy distribution in Z^0 decays using a new technique applied to a sample of inclusive B decays recorded in the SLD experiment at SLAC between 1996 and 1997. The upgraded CCD vertex detector is used to reconstruct B-decay vertices with high efficiency and purity, and to provide precise measurements of the kinematic quantities used in this technique. For each reconstructed B-decay vertex, the part of the B energy missing from the vertex is derived from the kinematic quantities. B vertices with low missing mass are selected to provide a very high purity sample and to obtain good energy resolution. We compare the scaled B hadron energy distribution with the predictions of several QCD and phenomenological models of heavy quark fragmention. The average scaled energy $< x_B >$ is measured to be 0.719 ± 0.005 (stat.)± 0.001 (unfolding) (preliminary).

Contributed to the XXIX International Conference on High Energy Physics, Vancouver, B.C. Canada, July 23-29 1998: Parallel session 3; plenary session 4.

*Work supported by Department of Energy contract DE-AC03-76SF00515 (SLAC).

1 Introduction

The production of heavy hadrons (H) in e^+e^- annihilation provides a laboratory for the study of heavy-quark (Q) jet fragmentation. This is commonly characterised in terms of the observable $x_H \equiv 2E_H/\sqrt{s}$, where E_H is the energy of a B or D hadron containing a b or c quark, respectively, and $\sqrt{s}$ is the c.m. energy. In contrast to light-quark jet fragmentation one expects [1] the distribution of x_H, $D(x_H)$, to peak at an x_H-value significantly above 0. Since the hadronisation process is intrinsically non-perturbative $D(x_H)$ cannot be calculated directly using perturbative Quantum Chromodynamics (QCD). However, the distribution of the closely-related variable $x_Q \equiv 2E_Q/\sqrt{s}$ can be calculated perturbatively [2, 3, 4] and related, via model-dependent assumptions, to the observable quantity $D(x_H)$; a number of such models of heavy quark fragmentation have been proposed [5, 6, 7]. Measurements of $D(x_H)$ thus serve to constrain both perturbative QCD and the model predictions. Furthermore, the measurement of $D(x_H)$ at different c.m. energies can be used to test QCD evolution, and comparison of $D(x_B)$ with $D(x_D)$ can be used to test heavy quark symmetry [8]. Finally, the uncertainty on the forms of $D(x_D)$ and $D(x_B)$ must be taken into account in studies of the production and decay of heavy quarks, see *eg.* [9]; more accurate measurements of these forms will allow increased precision in tests of the electroweak heavy-quark sector.

We consider measurement of the B hadron scaled energy distribution $D(x_B)$ in Z^0 decays. Earlier studies [10] used the momentum spectrum of the lepton from semi-leptonic B decays to constrain the mean value $< x_B >$ and found it to be approximately 0.70; this is in agreement with the results of similar studies at $\sqrt{s} = 29$ and 35 GeV [11]. In more recent analyses [12, 13, 14] the scaled energy distribution $D(x_B)$ has been measured by reconstructing B hadrons via their $B \rightarrow$ DlX decay mode. In this case the reconstruction efficiency is intrinsically low due to the small branching ratio for B hadrons to decay into the high-momentum leptons used in the tag. Also, the reconstruction of the B hadron energy using calorimeter information usually has

poor resolution for low B energy, resulting in poor sensitivity to the shape of the B hadron energy distribution at low energy.

Here we describe the preliminary results of a new method for reconstructing B hadron decays, and the B-energy, inclusively, using only charged tracks, in the SLD experiment at SLAC. We use the upgraded CCD vertex detector, installed in 1996, to reconstruct B-decay vertices with high efficiency and purity. Combined with the micron-size SLC interaction point (IP), precise vertexing allows us to reconstruct accurately the B flight direction and hence the transverse momentum of tracks associated with the vertex with respect to this direction. Using the transverse momentum and the total invariant mass of the associated tracks, an upper limit on the mass of the missing particles is found for each reconstructed B-decay vertex, and is used to solve for the longitudinal momentum of the missing particles, and hence for the energy of the B hadron. In order to improve the B sample purity and the reconstructed B hadron energy resolution, B vertices with low missing mass are selected. The method is described in Section 3. In Section 4 we compare the B energy distribution with the perturbative QCD and phenomenological model predictions.

2 Apparatus and Hadronic Event Selection

This analysis is based on roughly 150,000 hadronic events produced in e^+e^- annihilations at a mean center-of-mass energy of $\sqrt{s}$ = 91.28 GeV at the SLAC Linear Collider (SLC), and recorded in the SLC Large Detector (SLD) in 1996 and 1997. A general description of the SLD can be found elsewhere [15]. The trigger and initial selection criteria for hadronic Z^0 decays are described in Ref. [16]. This analysis used charged tracks measured in the Central Drift Chamber (CDC) [17] and in the upgraded Vertex Detector (VXD3) [18]. Momentum measurement is provided by a uniform axial magnetic field of 0.6T. The CDC and VXD3 give a momentum resolution of $\sigma_{p_\perp}/p_\perp = 0.01 \oplus 0.0026 p_\perp$, where $p_\perp$ is the track momentum transverse to the beam axis in

GeV/c. In the plane normal to the beamline the centroid of the micron-sized SLC IP was reconstructed from tracks in sets of approximately thirty sequential hadronic Z^0 decays to a precision of $\sigma^{r\phi} \simeq 7 \pm 2$ μm (1996) and $\sigma^{r\phi} \simeq 4 \pm 2$ μm (1997). The IP position along the beam axis was determined event by event using charged tracks with a resolution of $\sigma^z \simeq 35$ μm (1996) and $\sigma^z \simeq 30$ μm (1997). Including the uncertainty on the IP position, the resolution on the charged-track impact parameter (d) projected in the plane perpendicular to the beamline is $\sigma_d^{r\phi} = 14 \oplus 33/(p_\perp \sin^{3/2}\theta)$ μm (1996) and $\sigma_d^{r\phi} = 11 \oplus 33/(p_\perp \sin^{3/2}\theta)$ μm (1997), and the resolution in the plane containing the beam axis is $\sigma_d^z = 27 \oplus 33/(p_\perp \sin^{3/2}\theta)$ μm (1996) and $\sigma_d^z = 24 \oplus 33/(p_\perp \sin^{3/2}\theta)$ μm (1997), where θ is the track polar angle with respect to the beamline. The event thrust axis [19] was calculated using energy clusters measured in the Liquid Argon Calorimeter [20].

A set of cuts was applied to the data to select well-measured tracks and events well contained within the detector acceptance. Charged tracks were required to have a distance of closest approach transverse to the beam axis within 5 cm, and within 10 cm along the axis from the measured IP, as well as $|\cos\theta| < 0.80$, and $p_\perp > 0.15$ GeV/c. Events were required to have a minimum of seven such tracks, a thrust axis polar angle w.r.t. the beamline, θ_T, within $|\cos\theta_T| < 0.71$, and a charged visible energy E_{vis} of at least 20 GeV, which was calculated from the selected tracks assigned the charged pion mass. The efficiency for selecting a well-contained $Z^0 \to q\bar{q}(g)$ event was estimated to be above 96% independent of quark flavor. The selected sample comprised 111,569 events, with an estimated 0.10 ± 0.05% background contribution dominated by $Z^0 \to \tau^+\tau^-$ events.

For the purpose of estimating the efficiency and purity of the B hadron selection procedure we made use of a detailed Monte Carlo (MC) simulation of the detector. The-JETSET 7.4 [21] event generator was used, with parameter values tuned to hadronic e^+e^- annihilation data [22], combined with a simulation of B hadron decays tuned [23] to $\Upsilon(4S)$ data and a simulation of the SLD based on GEANT 3.21 [24]. Inclusive

distributions of single-particle and event-topology observables in hadronic events were found to be well described by the simulation [16]. Uncertainties in the simulation were taken into account in the systematic errors (Section 6).

3 B Hadron Selection and Energy Measurement

A B Hadron Selection

The B sample for this analysis is selected using a topological vertexing technique based on the detection and measurement of charged tracks, which is described in detail in Ref. [25]. Each hadronic event is divided into two hemispheres by a plane perpendicular to the thrust axis. In each hemisphere the topological vertexing algorithm is applied to the set of "quality" tracks having (i) at least 23 hits in the CDC and 2 hits in VXD3; (ii) a combined CDC and VXD3 track fit quality of χ^2/N_{dof} <8; (iii) a momentum in the range 0.25< p <55 GeV/c, (iv) an impact parameter of less than 0.3 cm in the $r\phi$ plane, and less than 1.5 cm along the z axis; (v) a transverse impact parameter error no larger than 250 μm.

Vertices consistent with photon conversions or K^0 and Λ decays are discarded. In hemispheres containing at least one found vertex the vertex furthest from the IP is retained as the 'seed' vertex. Those events were retained which contained a seed vertex separated from the IP by between 0.1 cm and 2.3 cm. The lower bound reduces contamination from non-B-decay tracks and backgrounds from light-flavor events, and the upper bound reduces the background from particle interactions with the beam pipe.

For each hemisphere containing an accepted seed vertex, a vertex axis is formed by the straight line joining the IP to the seed vertex, which is located at a distance D from the IP. For each quality track not directly associated with the vertex, the distance of closest approach to the vertex axis, T, and the distance from the IP along the vertex axis to the point of closest approach, L, are calculated. Tracks satisfying T< 1 mm

and L/D$>$ 0.3 are added to the vertex. These T and L cuts are chosen to minimize false track associations to the seed vertex, since the addition of a false track has a much greater kinematic effect than the omission of a genuine B-decay track, and hence has more effect on the reconstructed B hadron energy resolution. Our Monte Carlo studies show that, on average, this procedure attaches 0.85 tracks to each seed vertex. 91.9% of the tracks from tagged true B decays are associated with the resulting vertices, and 98.0% of the vertex tracks are from true B decays.

The large masses of the B hadrons relative to light-flavor hadrons make it possible to distinguish B hadron vertices from those found in events of light flavors using the vertex invariant mass, M. However, due to the missing particles, which are mainly neutrals, M cannot be fully determined. In the rest frame of the decaying hadron, M can be written as

$$M = \sqrt{M_{ch}^2 + P_t^2 + P_l^2} + \sqrt{M_0^2 + P_t^2 + P_l^2} \qquad (1)$$

where M_{ch} and M_0 are the total invariant masses of the set of vertex-associated tracks and missing particles, respectively, and P_t and P_l are the momenta transverse to and along the the vertex axis; P_t is calculated using the vertex-associated charged tracks. We use the lower bound on M, the 'P_t-corrected vertex mass',

$$M_{Pt} = \sqrt{M_{ch}^2 + P_t^2} + |P_t| \qquad (2)$$

as the basis for selecting B hadrons.

Figure 1 shows the distribution of the P_t-corrected vertex mass (points) for the 32,492 accepted hemispheres in the data sample, and the corresponding simulated distribution. The majority of non-B vertices have M_{Pt} less than 2.0 GeV/c^2. Therefore, to obtain a high purity B sample for this analysis, B hadron candidates are selected by requiring $M_{Pt} > 2.0$ GeV/c^2. We further required $M_{Pt} \leq 2 \times M_{ch}$ to reduce contaminations from fake vertices in light quark events. A total of 19,604 hemispheres are selected, with an estimated efficiency for selecting a true B-hemisphere of 40.1%, and a sample purity of 98.2%. The contributions from light-flavor events in the sample are 0.15% for primary u,d and s events and 1.6% for c events.

B B Hadron Energy Measurement

The energy of each B hadron, E_B, can be expressed as the sum of the reconstructed-vertex track energy, E_{ch}, and the energy of those particles not associated with the vertex, E_0. We can write E_0 as

$$E_0^2 = M_0^2 + P_t^2 + P_{0l}^2 \tag{3}$$

where P_{0l} is the net momentum along the vertex axis of the missing particles. E_{ch} is obtained directly by summing the energies of the associated tracks, assuming the charged pion mass for each track. To obtain E_0, the two unknowns, M_0 and P_{0l}, must be found. One kinematic constraint can be obtained by imposing the B hadron mass on the vertex, $M_B^2 = E_B^2 - P_B^2$, where $P_B = P_{chl} + P_{0l}$ is the total momentum of the B hadron, and P_{chl} is the momentum component of the associated tracks along the vertex axis. From this we derive the following inequality,

$$\sqrt{M_{ch}^2 + P_t^2} + \sqrt{M_0^2 + P_t^2} \leq M_B, \tag{4}$$

where equality holds in the limit where both P_{0l} and P_{chl} vanish in the B hadron rest frame. Equation (4) effectively sets an upper bound on M_0, and a lower bound is given by zero:

$$0 \leq M_0^2 \leq M_{0max}^2, \tag{5}$$

where

$$M_{0max}^2 = M_B^2 - 2M_B\sqrt{M_{ch}^2 + P_t^2} + M_{ch}^2. \tag{6}$$

Since M_0 is bounded from both above and below, we expect to obtain a good estimate of M_0, and therefore of the B hadron energy, when M_{0max} is small.

We have used our simulation to study this issue. Figure 2 shows the correlation between M_{0max} and the true M_0, M_{0true}, using simulated B^0 and $B^{\pm}$ decays, assuming $M_B = 5.28$ GeV/c^2. The true value of M_0 tends to cluster near its maximum value M_{0max}. This can be seen further in Figure 3, which shows the relative deviation of M_{0max} from M_{0true} for all B hadrons. Although approximately 25% of the B hadrons

are B_s^0 and Λ_b which have larger masses, the values of M_{0max} obtained using M_B=5.28 GeV/c^2 in Equation (6) are typically within about 10% of M_0. The distribution of the reconstructed M_{0max}^2 for vertices in the selected B hadron sample is shown in Figure 4. The simulation indicates that the non-$b\bar{b}$ background is concentrated at high M_{0max}^2; this because most of the light flavor vertices have small M_{Pt} and therefore, due to the strong negative correlation between M_{Pt} and M_{0max} shown in Figure 5, large M_{0max}. The negative tail in Figure 4 is an effect of detector resolution, and the Monte Carlo simulation shows good agreement with the data.

Because M_0 peaks near M_{0max}, we set $M_0^2 = M_{0max}^2$ if $M_{0max}^2 \geq 0$, and $M_0^2 = 0$ if $M_{0max}^2 < 0$. We then calculate P_{0l}:

$$P_{0l} = \frac{M_B^2 - (M_{ch}^2 + P_t^2) - (M_0^2 + P_t^2)}{2(M_{ch}^2 + P_t^2)} P_{chl}, \tag{7}$$

and hence E_0 (Equation (3)). We then divide the reconstructed B hadron energy, $E_B^{rec} = E_0 + E_{ch}$, by the beam energy, $E_{beam} = \sqrt{s}/2$, to obtain the reconstructed scaled B hadron energy, $x_B^{rec} = E_B^{rec}/E_{beam}$.

The resolution in x_B^{rec} depends on both M_{0max}^2 and the true x_B, x_B^{true}. Vertices in the negative tail of the M_{0max}^2 distribution that have $M_{0max}^2 < -1.0(GeV/c^2)^2$ are often poorly reconstructed and those with $M_{0max}^2 < -1$ are not used in further analysis. Vertices with small values of $|M_{0max}^2|$ are typically reconstructed with better resolution and an upper cut on M_{0max}^2 is hence applied. For an x_B-independent cut, the efficiency for selecting B hadrons is roughly linear in x_B^{true}. In order to obtain an approximately x_B-independent selection efficiency we chose the *ad hoc* upper cut:

$$M_{0max}^2 < (1.1 + 0.006(E_{beam} - E_B^{rec}) + 3.5exp(-(E_B^{rec} - 5.5)/3.5)^2, \tag{8}$$

where the two terms that depend on the reconstructed energy E_B^{rec} increase the efficiency at lower B hadron energy. Figure 6 shows the distribution of M_{0max}^2 after these cuts, where the data and Monte Carlo simulation are in good agreement.

About 0.7% of the selected vertices are from background light-flavor events, and they are concentrated in the lowest energy bin. To further remove these background

vertices, a vertex is required to contain at least 3 quality tracks with a normalized impact parameter greater than 2. This eliminates almost all of the u,d,s-event background and cuts the charm background by about 20% overall and 43% in the few lowest energy bins. This cut helps to reduce the dependence of the reconstructed B hadron energy distribution on light flavor Monte Carlo simulations in the low energy region, which is a key step towards finding the correct shape of the B hadron energy distribution at low energies.

A total of 1938 vertices in the data for 1996-97 satisfy all these selection cuts. Figure 7 shows the distribution of the reconstructed scaled B hadron energy for data, $D^{data}(x_B^{rec})$, and for the Monte Carlo simulation, $D^{MC}(x_B^{rec})$. The overall efficiency for selecting B hadrons is 3.95% and the estimated B hadron purity is 99.5%. The efficiency as a function of x_B^{true} is shown in Figure 8. The dependence is rather weak except for the lowest x_B region where the efficiency is about 1.7%. The Monte Carlo simulation predicts that among these vertices, about 0.06% are from u,d and s events and 0.46% are from charm events. The distribution of the background, $S(x_B^{rec})$, is also shown in Figure 7. These backgrounds are subtracted bin-by-bin from the $D^{data}(x_B^{rec})$ before we proceed to test various fragmentation models (see next section).

We examined the B-energy resolution of this technique. Figure 9 shows the distribution of the normalized difference between the true and reconstructed B hadron energies, $(x_B^{rec} - x_B^{true})/x_B^{true}$, for Monte Carlo events. The distribution is fitted by a double Gaussian, resulting in a core width (the width of the narrower Gaussian) of 10.4% and a tail width (the width of the wider Gaussian) of 23.6% with a core fraction of 83%. Figure 10 shows the core and tail widths as a function of x_B^{true}. In order to compare the widths from different x_B bins, we fixed the ratio between core and tail fractions to that obtained in the overall fit above. The x_B-dependence of the resolution is weak, although, as expected, the resolution is worse at lower B energies.

4 Comparison with Model Predictions

It is interesting to compare our measured B hadron energy distribution with the theoretical predictions. The event generator used in our simulation is based on a perturbative QCD 'parton shower' for production of quarks and gluons, together with the phenomenological Peterson function [6] (Table 1) to account for the fragmentation of b and c quarks into B and D hadrons, respectively, within the iterative Lund string hadronisation mechanism [21]; this simulation yields a generator-level primary B hadron energy distribution with $< x_B > = 0.693$*. It is apparent that this simulation does not reproduce the data well (Figure 7); the χ^2 for the comparison is 57.6 for 17 bins.

We have also considered alternative forms of the fragmentation function based on the phenomenological models of the Lund group [7] and of Kartvelishvili *et al.* [27], and the perturbative QCD calculations of Braaten *et al.*(BCFY) [4] and of Collins and Spiller [28], as well as *ad hoc* parametrisations based on a function used by the ALEPH Collaboration [12]. For the Collins and Spiller model, we have used the function derived assuming that the B-hadrons are leading, and are not produced by the decay of higher-mass resonances. For the purpose of exploring the characteristics of the shape of the fragmentation function, a 7th-order polynomial and a "power" function are also compared with the data. These functions are listed in Table 1. All models require that the distribution vanish at $x_B^{true} = 0$ and $x_B^{true} = 1$.

In order to make a consistent comparison of each function with the data we adopted the following procedure. Starting values of the arbitrary parameters were assigned and the corresponding distribution of scaled primary B hadron energies, $D^{MC}(x_B^{true})$, was reproduced in the MC-generated $b\bar{b}$ event sample, *before* simulation of the detector, by weighting events accordingly. The resulting distribution, after simulation of the detector, application of the analysis cuts and background subtraction, of reconstructed

*We used a value of the Peterson function parameter $\epsilon_b = 0.006$ [26].

B hadron energies, $D^{MC}(x_B^{rec})$, was then compared with the background-subtracted data distribution and the χ^2 value, defined as

$$\chi^2 = \sum_{i=1}^{N} \left(\frac{N_i^{data} - r N_i^{MC}}{\sigma_i} \right)^2 \tag{9}$$

was calculated, where N is the number of bins to be used in the comparison, N_i^{data} is the number of entries in bin i in the data distribution, and N_i^{MC} is the number of entries in bin i in the simulated distribution[†]. σ_i is the statistical error on the deviation of the observed number of entries for the data from the expected number of entries in bin i, which can be expressed as

$$\sigma_i^2 = \left(\sqrt{r N_i^{MC}} \right)^2 + \left(r \sqrt{N_i^{MC}} \right)^2, \tag{10}$$

where $\left(\sqrt{r N_i^{MC}} \right)^2$ is the expected statistical variance on the observed data in bin i, assuming the model being tested is correct, and $\left(r \sqrt{N_i^{MC}} \right)^2$ is the statistical variance on the expected number of entries in bin i.

The parameter values are then changed, the weighting process repeated in the simulated sample, and the new distribution of reconstructed B hadron energies compared with the data to yield a new χ^2 value. This process was iterated to find the minimum in χ^2, yielding a parameter set that gives an optimal description of the reconstructed data by the input fragmentation function.

Since the χ^2 test is not effective for bins with a very low number of entries, the third and the last three bins in Figure 7 are excluded from the fits. Also, in order to reduce the systematic dependence of our fit on the fragmentation function used in our default Monte Carlo simulation, we decided to exclude in addition the fourth bin in Figure 7 (the second bin that contains data), due to the low efficiency for that bin (Figure 8) where the fluctuation of Monte Carlo weights is relatively large. Data points excluded from the fit are represented in Figure 7 by open circles.

[†] r is the factor by which the total number of entries in the simulated distribution is scaled to the number of entries in the data distribution; $r \simeq 1/12$.

This procedure was applied for each function listed in Table 1. The fitted parameters and minimum χ^2 values are listed in Table 2, and the corresponding $D^{MC}(x_B^{rec})$ are compared with the data in Figure 11.

Among the phenomenological models, the Peterson function reproduces the data with a 5% χ^2 probability. The Kartvelishvili and Lund models do not reproduce the data because both models, especially the Lund model which contains an exponential factor, approach zero too fast as $x \to 0$. Neither of the two models based on perturbative QCD calculations (BCFY; Collins and Spiller) reproduces the data. We found two sets of parameters which optimize the ALEPH parametrization. "ALEPH 1", obtained by setting the parameter b (Table 1) to infinity, has a χ^2 probability of 43%, and "ALEPH 2", obtained by setting b to zero, has a χ^2 probability of 7%. Since the ALEPH parametrization is a generalized Peterson function with three parameters, we will retain it for further analysis. Similar to the Kartvelishvili model, the optimized "power" function, given by $x^{3.91}(1-x)^{0.894}$, also approaches zero very fast as $x \to 0$ and does not describe the data well. We considered *ad hoc* polynomials of different orders which vanish at both $x = 0$ and $x = 1$. At least a seventh-order polynomial is required to describe the data, resulting in a χ^2 of 14.4/12. However, such a multiparameter polynomial parametrisation is not based on any underlying physical model, and its behavior at low energies just outside the fitting range is unphysical, so we do not include the polynomial function in further analysis.

We conclude that, within our resolution and with our current data sample, we are able to distinguish between some of these functions. Kartvelishvili, Lund and our "power" function which are non-linear in x near $x = 0$ are disfavored. BCFY as well as Collins and Spiller are also disfavored because they have a larger width and lower peak than our data. "ALEPH 1" and "ALEPH 2" have acceptable χ^2 values. "ALEPH 1" which behaves like x as $x \to 0$ and $(1-x)$ as $x \to 1$ yielded the best χ^2 probability.

We should note, however, that fragmentation functions such as the Lund and Peterson functions were derived in terms of the variable $z = (E + p_{||})_H/(E + p||)_Q$, which

is not readily accessible experimentally. We have adopted the fraction of the beam energy carried by the hadron, $x = E_H/E_{beam}$, as the measured variable, which may somewhat alter the comparison with these models.

5 Correction of the B Energy Distribution

In order to compare our results with those from other experiments it is necessary to correct the reconstructed scaled B hadron energy distribution $D^{data}(x_B^{rec})$ for the effects of non-B backgrounds, detector acceptance, event selection and analysis bias, and initial-state radiation, as well as for bin-to-bin migration effects caused by the finite resolution of the detector and the analysis technique. We applied a 25×25 matrix unfolding procedure to $D^{data}(x_B^{rec})$ to obtain an estimate of the true distribution $D^{data}(x_B^{true})$:

$$D^{data}(x_B^{true}) \quad = \quad \epsilon^{-1}(x_B^{true}) \cdot E(x_B^{true}, x_B^{rec}) \cdot (D^{data}(x_B^{rec}) - S(x_B^{rec})) \qquad (11)$$

where S is a vector representing the background contribution, E is a matrix to correct for bin-to-bin migrations, and ϵ is a vector representing the efficiency for selecting true B hadron decays for the analysis.

The matrices S, E and ϵ were calculated from our MC simulation; the elements of ϵ are shown in Figure 8. The matrix E incorporates a convolution of the input fragmentation function with the resolution of the detector. $E(i,j)$ is the number of vertices with x_B^{true} in bin i and x_B^{rec} in bin j, normalized by the total number of vertices with x_B^{rec} in bin j. We evaluated E using the Monte Carlo simulation weighted according to an input fragmentation model. We used in turn the Peterson, Lund, Kartvelishvili, BCFY, Collins, ALEPH 1, ALEPH 2, and power functions, with the optimised parameters listed in Table 2, to produce both a generator-level input primary B hadron energy distribution $D^{MC}(x_B^{true})$, and a reconstructed distribution $D^{MC}(x_B^{rec})$, as discussed in the previous section. In each case E was evaluated by examining the population migrations of true B hadrons between bins of the input scaled B energy, x_B^{true}, and the

reconstructed scaled B energy, x_B^{rec}.

The data were then unfolded according to Equation (11) to yield $D^{data}(x_B^{true})$, which is shown for each input fragmentation function in Figure 12. It can be seen that the shapes of $D^{data}(x_B^{true})$ differ systematically among the assumed input fragmentation functions. These difference were used to assign systematic errors, as discussed in the next section.

6 Systematic Errors

We have considered sources of systematic uncertainty that potentially affect our measurement of the B hadron energy distribution. These may be divided into uncertainties in modelling the detector and uncertainties on experimental measurements serving as input parameters to the underlying physics modelling. For these studies our standard simulation, employing the Peterson fragmentation function, was used. This study is in progress and we expect smaller or comparable systematic errors to our previous published result [14].

The model-dependence of the unfolding procedure was estimated by considering the envelope of the unfolded results illustrated in Figure 12. Since only ALEPH 1, ALEPH 2, and Peterson provide an acceptable χ^2 probablity in fitting to the data, in each bin of x_B we calculated the average value of these three unfolded results as well as the r.m.s. deviation. The average value was taken as our central value in each bin, and the r.m.s. value was assigned as the respective unfolding uncertainty.

7 Summary and Conclusions

We have used the precise SLD tracking system to reconstruct the energies of B hadrons in $e^+e^- \to Z^0$ events using an inclusive sample of B hadrons. We estimate our resolution on the B energy to be about 10.4% for roughly 83% of the reconstructed decays. The distribution of reconstructed scaled B hadron energy, $D(x_B^{rec})$, was compared with

perturbative QCD and phenomenological model predictions; the Peterson function and the *ad hoc* parametrization used by ALEPH are consistent with our data. The phenomenological models of the Lund group and of Kartvelishvili *et al.*, and the models based on the perturbative QCD calculations of Braaten *et al.* and of Collins and Spiller are not consistent with our data. The distribution was then corrected for bin-to-bin migrations caused by the resolution of the method and for selection efficiency to derive the energy distribution of primary B hadrons produced in Z^0 decays. Systematic uncertainties in the correction have not yet been considered, but we expect them to be smaller than, or comparable with, our previous published result [14]. The final corrected x_B distribution $D(x_B)$ is shown in Figure 13; the statistical and unfolding uncertainties are indicated separately.

It is conventional to evaluate the mean of this distribution, $< x_B >$. For each of the three functions providing a reasonable description of the data we evaluated $< x_B >$ from the distribution that corresponds to the optimised parameters; these are listed in Table 2. We took the average of the three values of $< x_B >$ as the central result, and defined the unfolding uncertainty to be the r.m.s. deviation. Other systematic errors have not yet been included. We obtained:

$$< x_B > \quad = \quad 0.719 \pm 0.005(stat.) \pm 0.001(unfolding), \tag{12}$$

which is consistent with previous measurements ([10], [12], [13] and [14]). It can be seen that $< x_B >$ is relatively insensitive to the variety of allowed forms of the shape of the fragmentation function $D(x_B)$.

Acknowledgements

We thank the personnel of the SLAC accelerator department and the technical staffs of our collaborating institutions for their outstanding efforts on our behalf.

*Work supported by Department of Energy contracts: DE-FG02-91ER40676 (BU), DE-FG03-91ER40618 (UCSB), DE-FG03-92ER40689 (UCSC), DE-FG03-93ER40788 (CSU), DE-FG02-91ER40672 (Colorado), DE-FG02-91ER40677 (Illinois), DE-AC03-76SF00098 (LBL), DE-FG02-92ER40715 (Massachusetts), DE-FC02-94ER40818 (MIT), DE-FG03-96ER40969 (Oregon), DE-AC03-76SF00515 (SLAC), DE-FG05-91ER40627 (Tennessee), DE-FG02-95ER40896 (Wisconsin), DE-FG02-92ER40704 (Yale); National Science Foundation grants: PHY-91-13428 (UCSC), PHY-89-21320 (Columbia), PHY-92-04239 (Cincinnati), PHY-95-10439 (Rutgers), PHY-88-19316 (Vanderbilt), PHY-92-03212 (Washington); The UK Particle Physics and Astronomy Research Council (Brunel, Oxford and RAL); The Istituto Nazionale di Fisica Nucleare of Italy (Bologna, Ferrara, Frascati, Pisa, Padova, Perugia); The Japan-US Cooperative Research Project on High Energy Physics (Nagoya, Tohoku); The Korea Research Foundation (Soongsil, 1997).

References

[1] See e.g. J.D. Bjorken, Phys. Rev. **D17** (1978) 171.

[2] B. Mele and P. Nason, Phys. Lett. **B245** (1990) 635.
B. Mele and P. Nason, Nucl. Phys. **B361** (1991) 626.
G. Colangelo and P. Nason, Phys. Lett. **B285** (1992) 167.

[3] Yu. L. Dokshitzer, V.A. Khoze, S.I. Troyan, Phys. Rev. **D53** (1996) 89.

[4] E. Braaten, K. Cheung, T.C. Yuan, Phys. Rev. **D48** (1993) R5049.
E. Braaten, K. Cheung, S. Fleming, T.C. Yuan, Phys. Rev. **D51** (1995) 4819.

[5] M.G. Bowler, Z. Phys. **C11** (1981) 169.

[6] C. Peterson, D. Schlatter, I. Schmitt and P.M. Zerwas, Phys. Rev. **D27** (1983) 105.

[7] B. Andersson, G. Gustafson, G. Ingelman, T. Sjöstrand, Phys. Rep. **97** (1983) 32.

[8] L. Randall, N. Rius, Nucl. Phys. **B441** (1995) 167.

[9] The LEP Electroweak Working Group, D. Abbaneo *et al.*, LEPHF/96-01 (July 1996).

[10] ALEPH Collab., D. Buskulic *et al.*, Z. Phys. **C62** (1994) 179.
DELPHI Collab., P. Abreu *et al.*, Z. Phys. **C66** (1995) 323.
L3 Collab., O. Adeva *et al.*, Phys Lett. **B261** (1991) 177.
OPAL Collab., P.D. Acton *et al.*, Z. Phys. **C60** (1993) 199.

[11] See e.g. D.H. Saxon in 'High Energy Electron-Positron Physics', Eds. A. Ali, P. Söding, World Scientific 1988, p. 539.

[12] ALEPH Collab., D. Buskulic *et al.*, Phys. Lett. **B357** (1995) 699.

[13] OPAL Collab., G. Alexander *et al.*, Phys. Lett. **B364** (1995) 93.

[14] SLD Collab., K. Abe *et al.*, Phys. Rev. **D56** (1997) 5310.

[15] SLD Design Report, SLAC Report 273 (1984).

[16] SLD Collaboration, K. Abe *et al.*, Phys. Rev. **D51** (1995) 962.

[17] M.D. Hildreth *et al.*, IEEE Trans. Nucl. Sci. **42** (1994) 451.

[18] C.J.S. Damerell et. al., Nucl. Instr. Meth. **A400** (1997) 287.

[19] S. Brandt *et al.*, Phys. Lett. **12** (1964) 57.
E. Farhi, Phys. Rev. Lett. **39** (1977) 1587.

[20] D. Axen *et al.*, Nucl. Inst. Meth. **A328** (1993) 472.

[21] T. Sjöstrand, Comput. Phys. Commun. **82** (1994) 74.

[22] P. N. Burrows, Z. Phys. **C41** (1988) 375.
OPAL Collab., M.Z. Akrawy *et al.*, Z. Phys. **C47** (1990) 505.

[23] SLD Collab., K. Abe *et al.*, SLAC-PUB-7117; to appear in Phys. Rev. Lett.

[24] R. Brun *et al.*, Report No. CERN-DD/EE/84-1 (1989).

[25] D. J. Jackson, Nucl. Inst. and Meth. **A388**, 247 (1997).

[26] SLD Collab., K. Abe *et al.*, Phys. Rev. **D53** (1996) 1023.

[27] V. G. Kartvelishvili, A. K. Likhoded and V. A. Petrov, Phys. Lett. **78B** (1978) 615.

[28] P.D.B. Collins and T.P. Spiller, J. Phys. G **11** (1985) 1289.

**List of Authors

K. Abe,[2] K. Abe,[19] T. Abe,[27] I.Adam,[27] T. Akagi,[27] N. J. Allen,[4]
A. Arodzero,[20] W.W. Ash,[27] D. Aston,[27] K.G. Baird,[15] C. Baltay,[37]
H.R. Band,[36] M.B. Barakat,[14] O. Bardon,[17] T.L. Barklow,[27] J.M. Bauer,[16]
G. Bellodi,[21] R. Ben-David,[37] A.C. Benvenuti,[3] G.M. Bilei,[23] D. Bisello,[22]
G. Blaylock,[15] J.R. Bogart,[27] B. Bolen,[16] G.R. Bower,[27] J. E. Brau,[20]
M. Breidenbach,[27] W.M. Bugg,[30] D. Burke,[27] T.H. Burnett,[35] P.N. Burrows,[21]
A. Calcaterra,[11] D.O. Caldwell,[32] D. Calloway,[27] B. Camanzi,[10]
M. Carpinelli,[24] R. Cassell,[27] R. Castaldi,[24] A. Castro,[22] M. Cavalli-Sforza,[33]
A. Chou,[27] E. Church,[35] H.O. Cohn,[30] J.A. Coller,[5] M.R. Convery,[27]
V. Cook,[35] R. Cotton,[4] R.F. Cowan,[17] D.G. Coyne,[33] G. Crawford,[27]
C.J.S. Damerell,[25] M. N. Danielson,[7] M. Daoudi,[27] N. de Groot,[27]
R. Dell'Orso,[23] P.J. Dervan,[4] R. de Sangro,[11] M. Dima,[9] A. D'Oliveira,[6]
D.N. Dong,[17] P.Y.C. Du,[30] R. Dubois,[27] B.I. Eisenstein,[12] V. Eschenburg,[16]
E. Etzion,[36] S. Fahey,[7] D. Falciai,[11] C. Fan,[7] J.P. Fernandez,[33] M.J. Fero,[17]
K.Flood,[15] R. Frey,[20] T. Gillman,[25] G. Gladding,[12] S. Gonzalez,[17]
E.L. Hart,[30] J.L. Harton,[9] A. Hasan,[4] K. Hasuko,[31] S. J. Hedges,[5]
S.S. Hertzbach,[15] M.D. Hildreth,[27] J. Huber,[20] M.E. Huffer,[27] E.W. Hughes,[27]
X.Huynh,[27] H. Hwang,[20] M. Iwasaki,[20] D. J. Jackson,[25] P. Jacques,[26]
J.A. Jaros,[27] Z.Y. Jiang,[27] A.S. Johnson,[27] J.R. Johnson,[36] R.A. Johnson,[6]
T. Junk,[27] R. Kajikawa,[19] M. Kalelkar,[26] Y. Kamyshkov,[30] H.J. Kang,[26]
I. Karliner,[12] H. Kawahara,[27] Y. D. Kim,[28] R. King,[27] M.E. King,[27]
R.R. Kofler,[15] N.M. Krishna,[7] R.S. Kroeger,[16] M. Langston,[20] A. Lath,[17]

D.W.G. Leith,[27] V. Lia,[17] C.-J. S. Lin,[27] X. Liu,[33] M.X. Liu,[37] M. Loreti,[22] A. Lu,[32] H.L. Lynch,[27] J. Ma,[35] G. Mancinelli,[26] S. Manly,[37] G. Mantovani,[23] T.W. Markiewicz,[27] T. Maruyama,[27] H. Masuda,[27] E. Mazzucato,[10] A.K. McKemey,[4] B.T. Meadows,[6] G. Menegatti,[10] R. Messner,[27] P.M. Mockett,[35] K.C. Moffeit,[27] T.B. Moore,[37] M.Morii,[27] D. Muller,[27] V.Murzin,[18] T. Nagamine,[31] S. Narita,[31] U. Nauenberg,[7] H. Neal,[27] M. Nussbaum,[6] N.Oishi,[19] D. Onoprienko,[30] L.S. Osborne,[17] R.S. Panvini,[34] H. Park,[20] C. H. Park,[29] T.J. Pavel,[27] I. Peruzzi,[11] M. Piccolo,[11] L. Piemontese,[10] E. Pieroni,[24] K.T. Pitts,[20] R.J. Plano,[26] R. Prepost,[36] C.Y. Prescott,[27] G.D. Punkar,[27] J. Quigley,[17] B.N. Ratcliff,[27] T.W. Reeves,[34] J. Reidy,[16] P.L. Reinertsen,[33] P.E. Rensing,[27] L.S. Rochester,[27] P.C. Rowson,[8] J.J. Russell,[27] O.H. Saxton,[27] T. Schalk,[33] R.H. Schindler,[27] B.A. Schumm,[33] J. Schwiening,[27] S. Sen,[37] V.V. Serbo,[36] M.H. Shaevitz,[8] J.T. Shank,[5] G. Shapiro,[13] D.J. Sherden,[27] K. D. Shmakov,[30] C. Simopoulos,[27] N.B. Sinev,[20] S.R. Smith,[27] M. B. Smy,[9] J.A. Snyder,[37] H. Staengle,[9] A. Stahl,[27] P. Stamer,[26] R. Steiner,[1] H. Steiner,[13] M.G. Strauss,[15] D. Su,[27] F. Suekane,[31] A. Sugiyama,[19] S. Suzuki,[19] M. Swartz,[27] A. Szumilo,[35] T. Takahashi,[27] F.E. Taylor,[17] J. Thom,[27] E. Torrence,[17] N. K. Toumbas,[27] A.I. Trandafir,[15] J.D. Turk,[37] T. Usher,[27] C. Vannini,[24] J. Va'vra,[27] E. Vella,[27] J.P. Venuti,[34] R. Verdier,[17] P.G. Verdini,[24] S.R. Wagner,[27] D. L. Wagner,[7] A.P. Waite,[27] Walston, S.,[20] J.Wang,[27] C. Ward,[4] S.J. Watts,[4] A.W. Weidemann,[30] E. R. Weiss,[35] J.S. Whitaker,[5] S.L. White,[30] F.J. Wickens,[25] B. Williams,[7] D.C. Williams,[17] S.H. Williams,[27] S. Willocq,[27] R.J. Wilson,[9] W.J. Wisniewski,[27] J. L. Wittlin,[15] M. Woods,[27] G.B. Word,[34] T.R. Wright,[36] J. Wyss,[22] R.K. Yamamoto,[17] J.M. Yamartino,[17] X. Yang,[20] J. Yashima,[31] S.J. Yellin,[32] C.C. Young,[27] H. Yuta,[2] G. Zapalac,[36] R.W. Zdarko,[27] J. Zhou.[20]

(The SLD Collaboration)

[1] *Adelphi University, South Avenue- Garden City,NY 11530,*
[2] *Aomori University, 2-3-1 Kohata, Aomori City, 030 Japan,*
[3] *INFN Sezione di Bologna, Via Irnerio 46 I-40126 Bologna (Italy),*
[4] *Brunel University, Uxbridge, Middlesex - UB8 3PH United Kingdom,*
[5] *Boston University, 590 Commonwealth Ave. - Boston,MA 02215,*
[6] *University of Cincinnati, Cincinnati,OH 45221,*
[7] *University of Colorado, Campus Box 390 - Boulder,CO 80309,*
[8] *Columbia University, Nevis Laboratories P.O.Box 137 - Irvington,NY 10533,*
[9] *Colorado State University, Ft. Collins,CO 80523,*

[10] *INFN Sezione di Ferrara, Via Paradiso,12 - I-44100 Ferrara (Italy),*
[11] *Lab. Nazionali di Frascati, Casella Postale 13 I-00044 Frascati (Italy),*
[12] *University of Illinois, 1110 West Green St. Urbana,IL 61801,*
[13] *Lawrence Berkeley Laboratory, Dept.of Physics 50B-5211 University of California-Berkeley,CA 94720,*
[14] *Louisiana Technical University, ,*
[15] *University of Massachusetts, Amherst,MA 01003,*
[16] *University of Mississippi, University,MS 38677,*
[17] *Massachusetts Institute of Technology, 77 Massachussetts Avenue Cambridge,MA 02139,*
[18] *Moscow State University, Institute of Nuclear Physics 119899 Moscow Russia,*
[19] *Nagoya University, Nagoya 464 Japan,*
[20] *University of Oregon, Department of Physics Eugene,OR 97403,*
[21] *Oxford University, Oxford, OX1 3RH, United Kingdom,*
[22] *Universita di Padova, Via F. Marzolo,8 I-35100 Padova (Italy),*
[23] *Universita di Perugia, Sezione INFN, Via A. Pascoli I-06100 Perugia (Italy),*
[24] *INFN, Sezione di Pisa, Via Livornese,582/AS Piero a Grado I-56010 Pisa (Italy),*
[25] *Rutherford Appleton Laboratory, Chiton,Didcot - Oxon OX11 0QX United Kingdom,*
[26] *Rutgers University, Serin Physics Labs Piscataway,NJ 08855-0849,*
[27] *Stanford Linear Accelerator Center, 2575 Sand Hill Road Menlo Park,CA 94025,*
[28] *Sogang University, Ricci Hall Seoul, Korea,*
[29] *Soongsil University, Dongjakgu Sangdo 5 dong 1-1 Seoul, Korea 156-743,*
[30] *University of Tennessee, 401 A.H. Nielsen Physics Blg. - Knoxville,Tennessee 37996-1200,*
[31] *Tohoku University, Bubble Chamber Lab. - Aramaki - Sendai 980 (Japan),*
[32] *U.C. Santa Barbara, 3019 Broida Hall Santa Barbara,CA 93106,*
[33] *U.C. Santa Cruz, Santa Cruz,CA 95064,*
[34] *Vanderbilt University, Stevenson Center,Room 5333 P.O.Box 1807,Station B Nashville,TN 37235,*
[35] *University of Washington, Seattle,WA 98105,*
[36] *University of Wisconsin, 1150 University Avenue Madison,WS 53706,*
[37] *Yale University, 5th Floor Gibbs Lab. - P.O.Box 208121 - New Haven,CT 06520-8121.*

Table 1: Fragmentation functions used in comparison with the data. For the BCFY function $f_1(r) = 3(3-4r)$, $f_2(r) = 12-23r+26r^2$, $f_3(r) = (1-r)(9-11r+12r^2)$, and $f_4(r) = 3(1-r)^2(1-r+r^2)$. A polynomial function and a power function are also included (see text for discussion).

Function	$D(x)$	Reference
ALEPH	$\frac{1+b(1-x)}{x}(1-\frac{c}{x}-\frac{d}{1-x})^{-2}$	[12]
BCFY	$\frac{x(1-x)^2}{[1-(1-r)x]^6}[3+\sum_{i=1}^{4}(-x)^i f_i(r)]$	[4]
Collins and Spiller	$(\frac{1-x}{x}+\frac{(2-x)\epsilon_b}{1-x})(1+x^2)(1-\frac{1}{x}-\frac{\epsilon_b}{1-x})^{-2}$	[28]
Kartvelishvili *et al.*	$x^{\alpha_b}(1-x)$	[27]
Lund	$\frac{1}{x}(1-x)^a exp(-bm_\perp^2/x)$	[7]
Peterson *et al.*	$\frac{1}{x}(1-\frac{1}{x}-\frac{\epsilon_b}{1-x})^{-2}$	[6]
Polynomial	$x(1-x)(1+\sum_{i=1}^{5}p_i x^i)$	(see text)
Power	$x^\alpha(1-x)^\beta$	(see text)

Table 2: Results of the χ^2 fit of fragmentation functions to the reconstructed B hadron energy distribution after background substraction. Minimum χ^2, number of degrees of freedom and coresponding parameter values are listed. Errors are statistical only.

Function	χ^2/dof	Parameters	$\langle x_B \rangle$
ALEPH 1	15.2/15	$c = 0.860^{+0.019}_{-0.018}$	0.718±0.005
		$d = 0.019 \pm 0.002$	
ALEPH 2	23.7/15	$c = 0.938^{+0.039}_{-0.034}$	0.720±0.005
		$d = 0.036 \pm 0.002$	
BCFY	52.3/16	$r = 0.2316^{+0.0092}_{-0.0088}$	0.713±0.005
Collins and Spiller	54.3/16	$\epsilon_b = 0.044^{+0.005}_{-0.004}$	0.714±0.005
Kartvelishvili *et al.*	79.6/16	$\alpha_b = 4.15 \pm 0.11$	0.720±0.004
Lund	139.1/15	$a = 2.116^{+0.118}_{-0.114}$	0.720±0.005
		$bm_\perp^2 = 0.408^{+0.073}_{-0.070}$	
Peterson *et al.*	26.0/16	$\epsilon_b = 0.0338^{+0.0020}_{-0.0022}$	0.719±0.005
Polynomial	14.4/12	$p_1 = -12.4 \pm 0.4$	(see text)
		$p_2 = 58.7 \pm 1.9$	
		$p_3 = -130.5 \pm 4.2$	
		$p_4 = 136.8 \pm 4.3$	
		$p_5 = -53.7 \pm 1.8$	
Power	78.5/15	$\alpha = 3.91^{+0.25}_{-0.24}$	0.722±0.005
		$\beta = 0.894^{+0.102}_{-0.097}$	

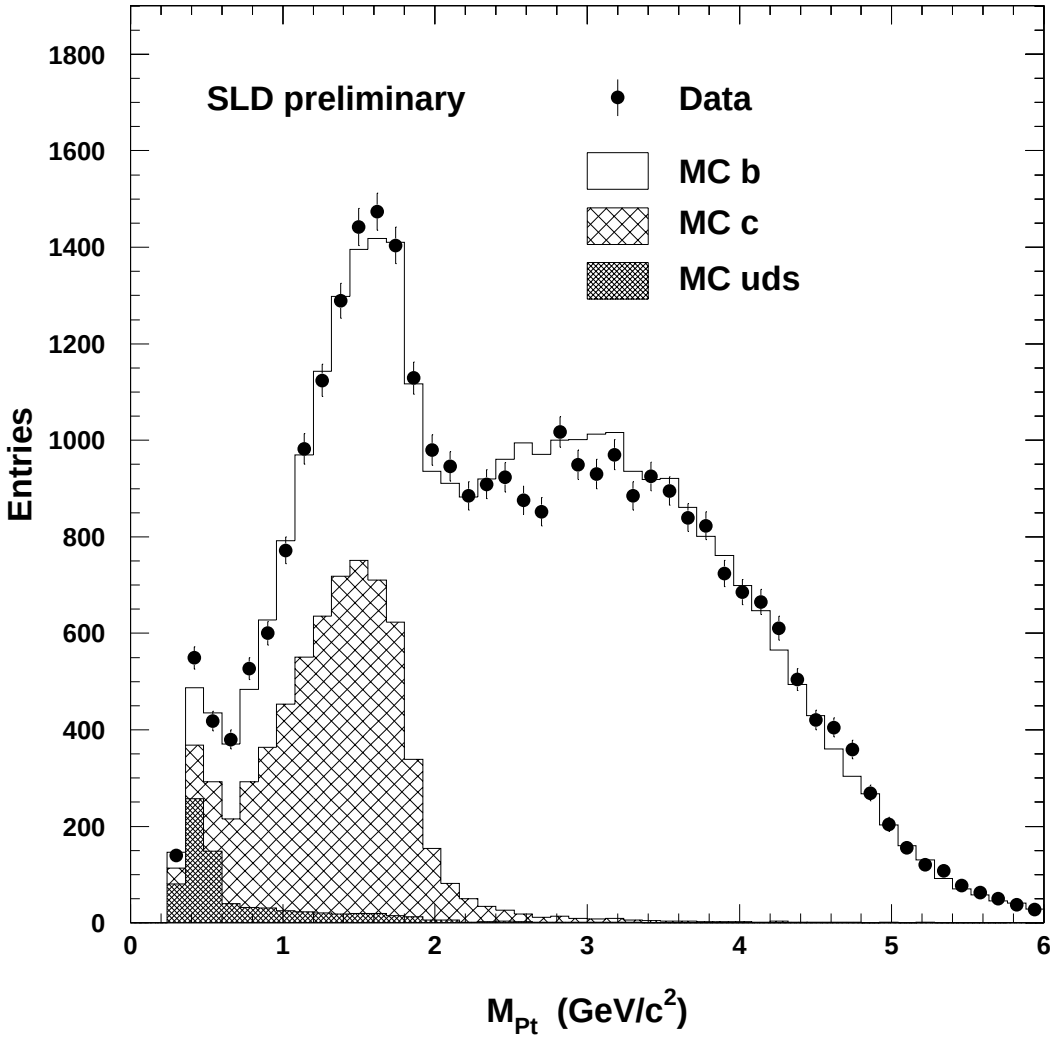

Figure 1: Distribution of the reconstructed P_t-corrected vertex mass in the 1996-97 data (points). Also shown is the prediction of the Monte Carlo simulation, for which the flavor composition is indicated.

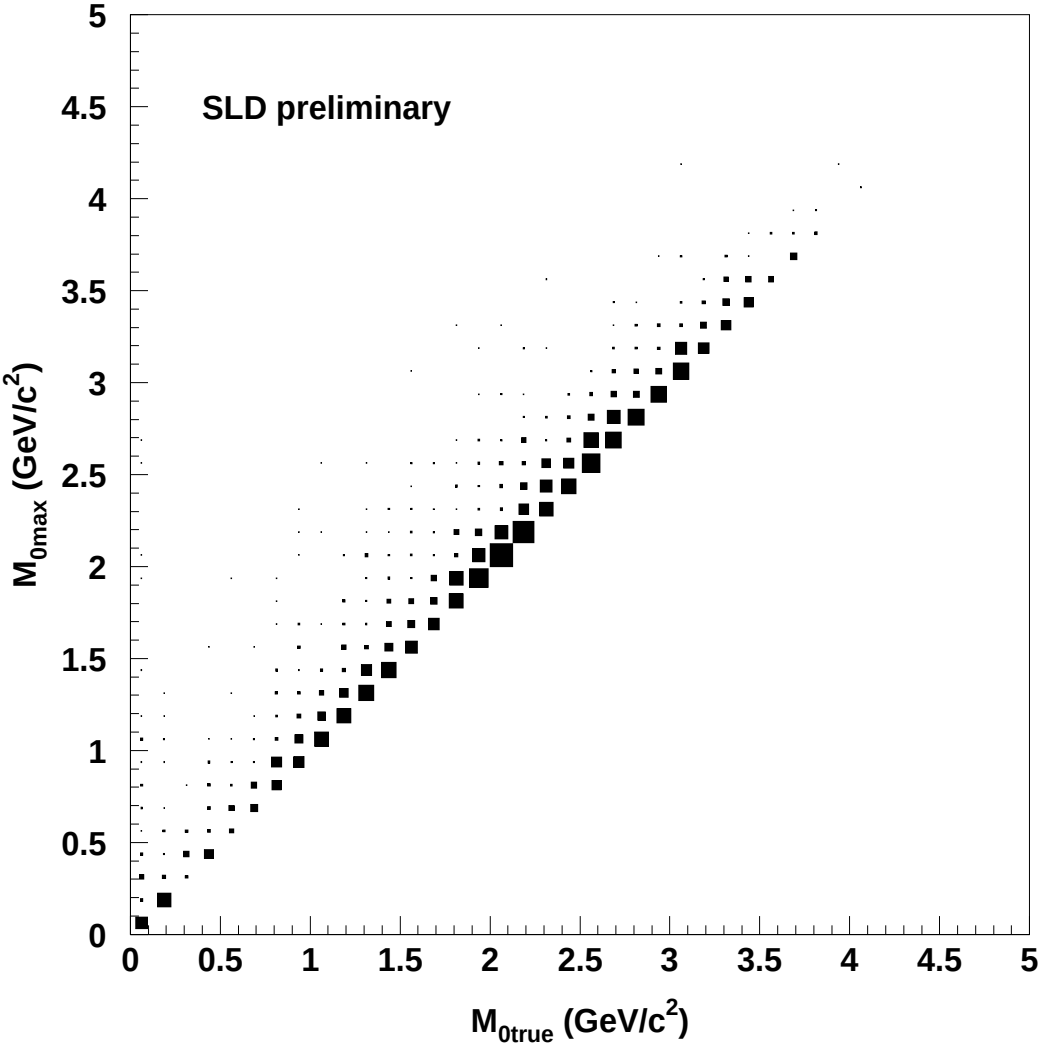

Figure 2: Correlation between the maximum missing mass (see text) and the true missing mass in Monte Carlo simulated B^0 and $B^{\pm}$ hadron decays.

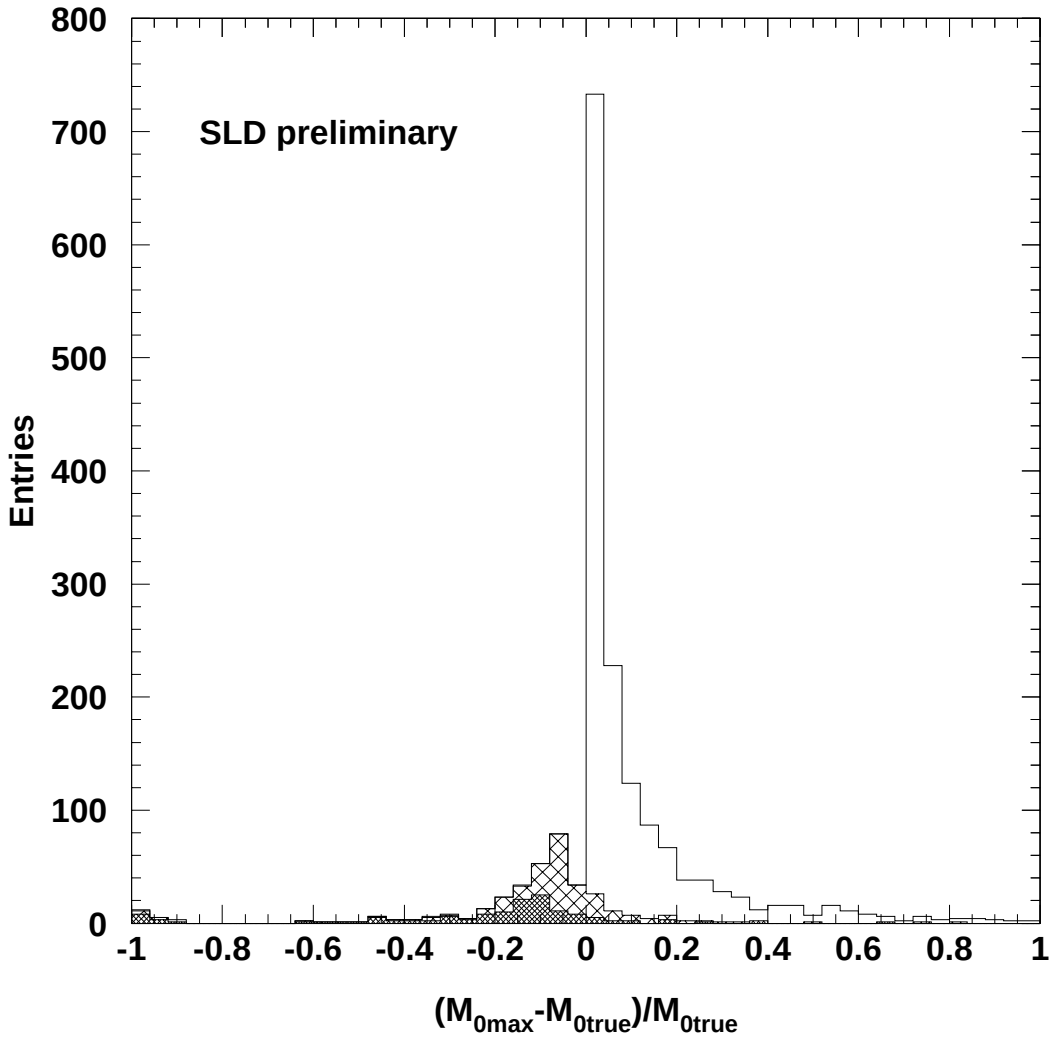

Figure 3: The relative deviation of the maximum missing mass from the true missing mass for Monte Carlo simulated B hadron decays, which is divided into three categories: B^0 and $B^{\pm}$ (open), B_s^0 (cross-hatched), and Λ_b (dark hatched).

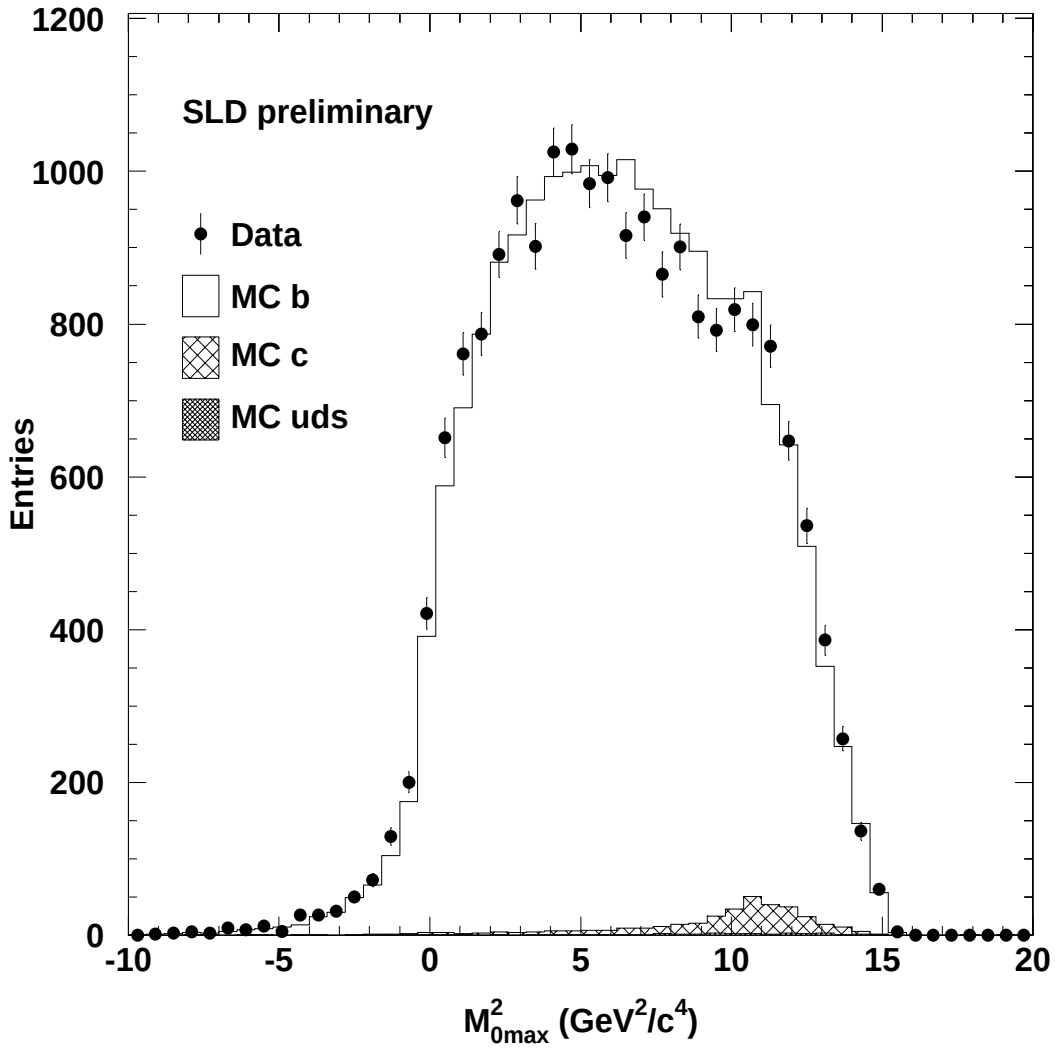

Figure 4: Distribution of the reconstructed M^2_{0max} for the selected vertices in the 1996-97 data (points). Also shown is the prediction of the Monte Carlo simulation.

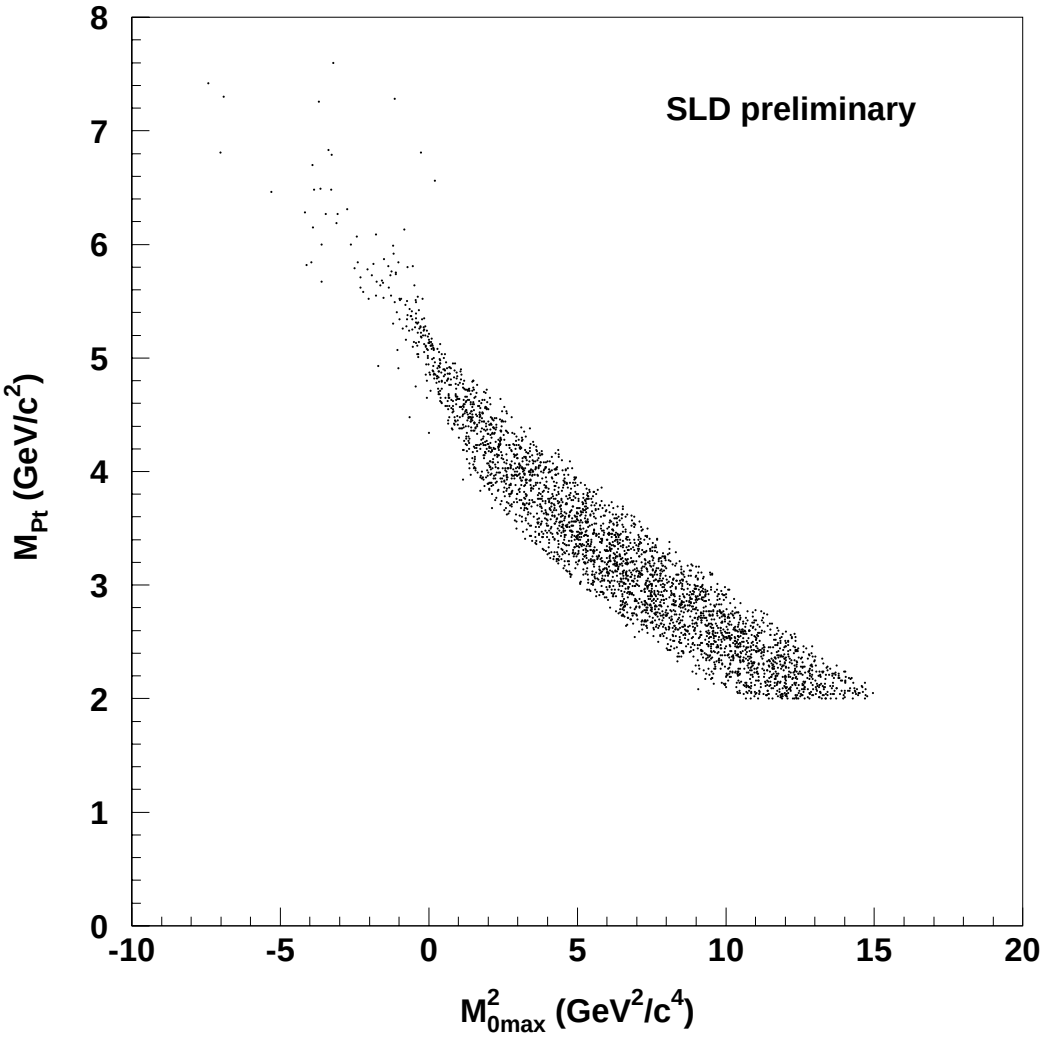

Figure 5: Correlation between M_{Pt} and M^2_{0max} for reconstructed B hadron vertices in the Monte Carlo simulation.

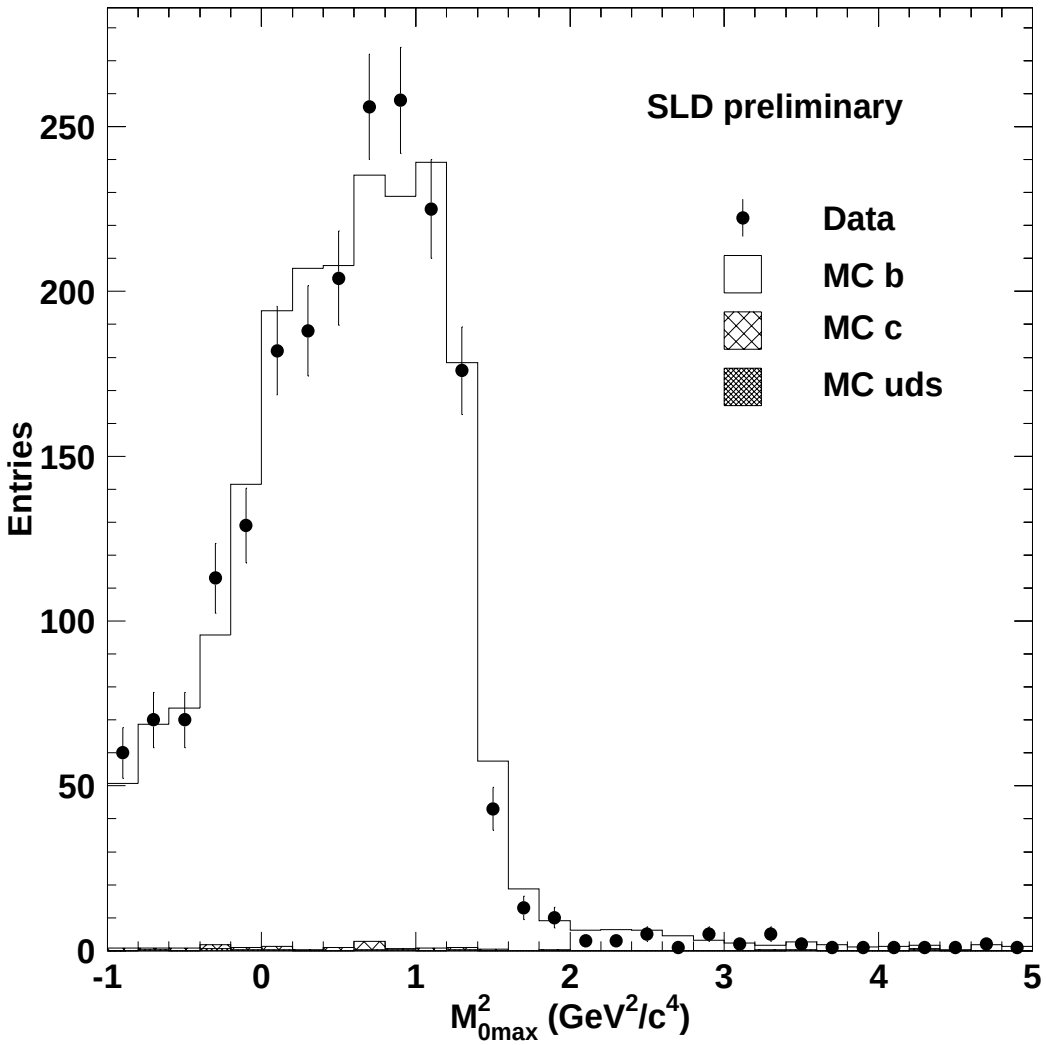

Figure 6: Distribution of the reconstructed M^2_{0max} for the final selected B sample (see text). Also shown is the prediction of the Monte Carlo simulation.

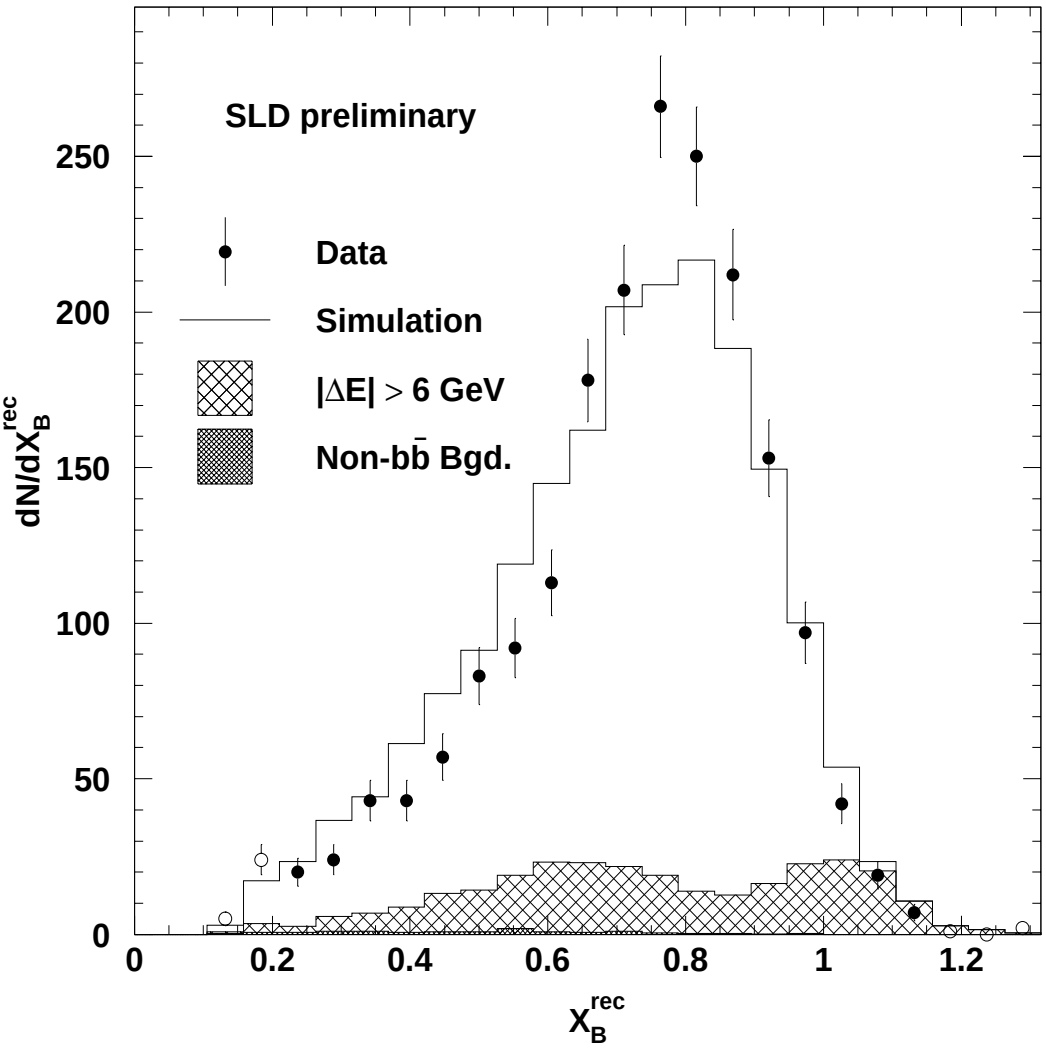

Figure 7: Distribution of the reconstructed scaled B hadron energy for data (points) and Monte Carlo (histogram). The cross-hatched histogram shows the distribution for cases with a 6 GeV or more deviation of the reconstructed energy from the true energy. The solid histogram shows the non-$b\bar{b}$ background.

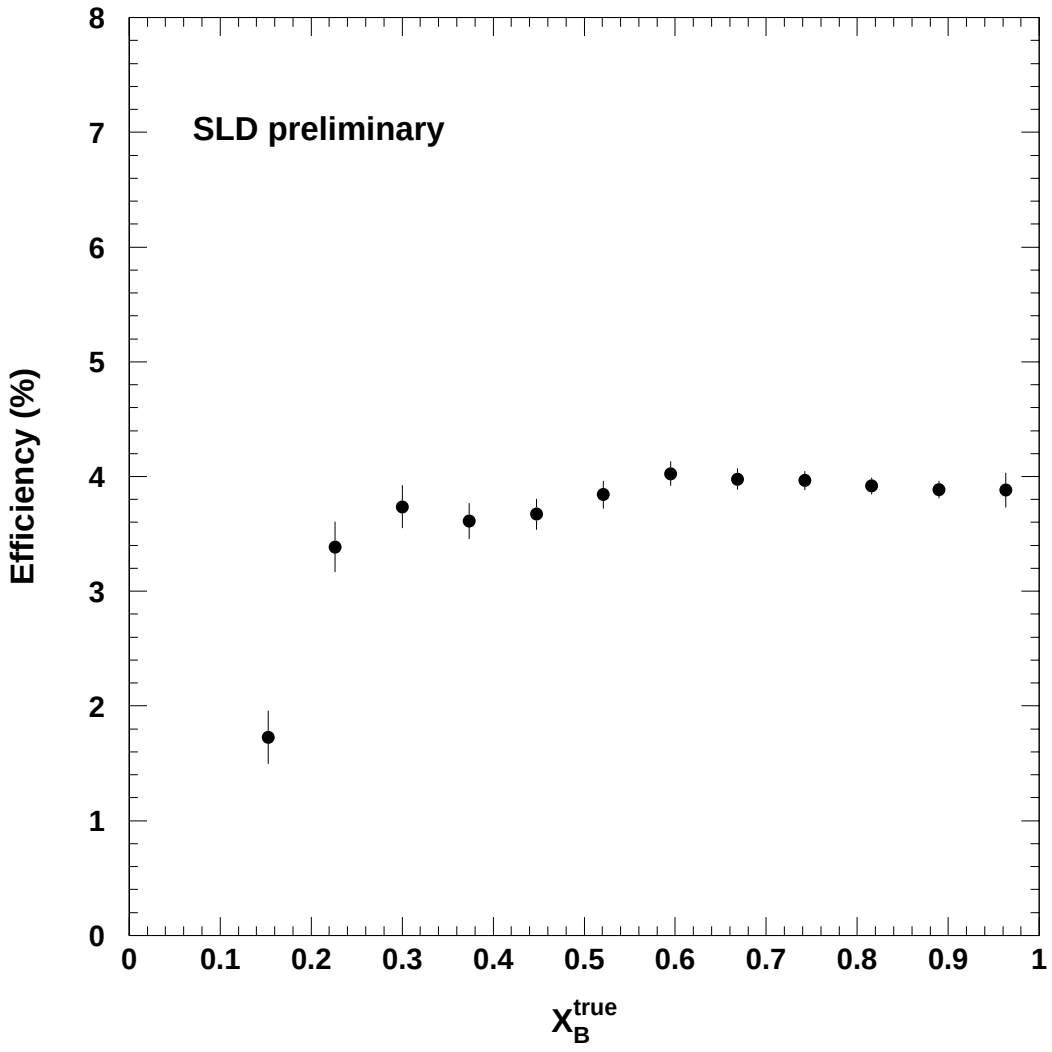

Figure 8: The Monte Carlo simulated efficiency for selecting B hadron decay vertices as a function of the true scaled B hadron energy, $x^{true} = E_B^{true}/E_{beam}$.

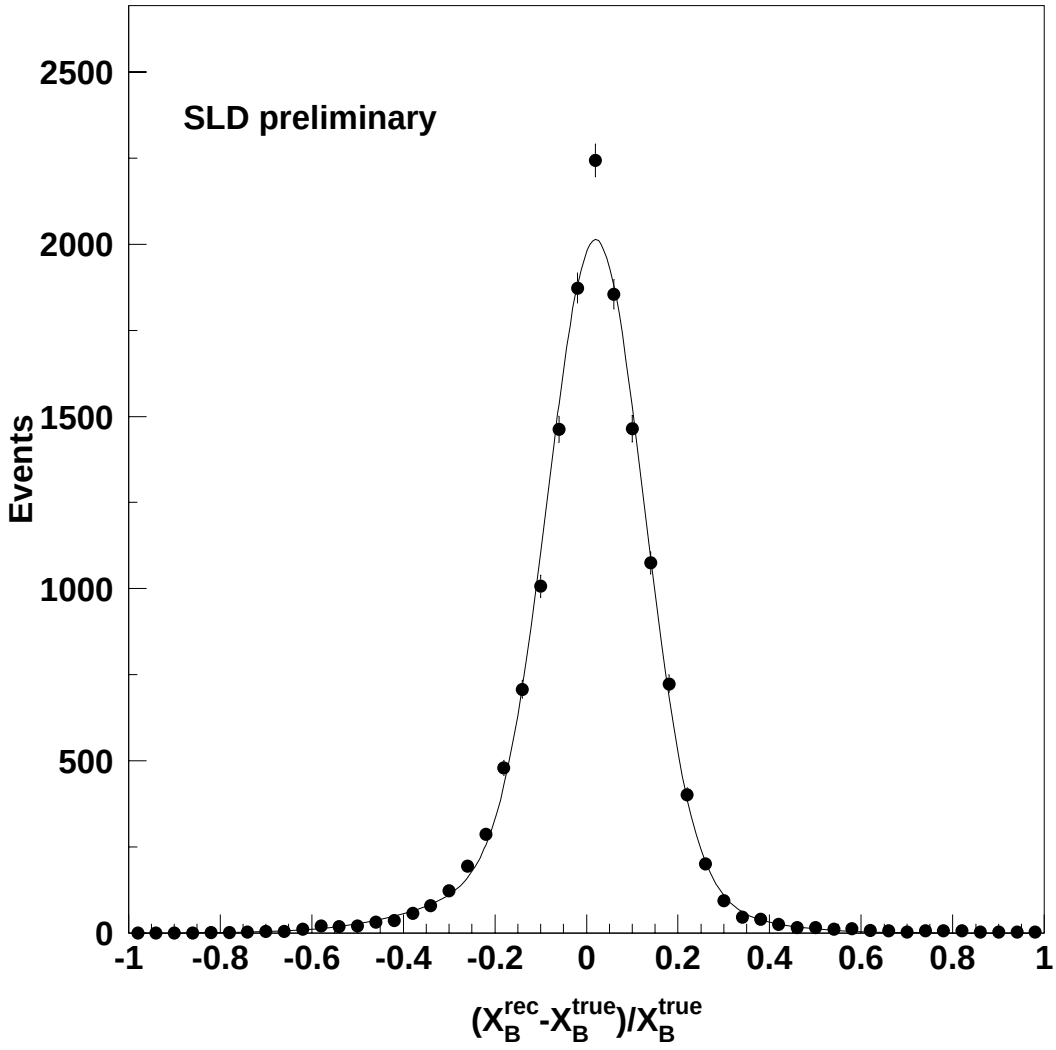

Figure 9: Distribution of the normalised difference between the reconstructed and true B energies for Monte Carlo simulated B vertices passing all cuts (points). The curve represents the result of a double Gaussian fit to the distribution. The resulting ratio of the amplitude of the inner Gaussian (core) to that of the outer Gaussian (tail) is 83:17, and the resulting widths are 10.4% for the core distribution, and 23.6% for the tail distribution.

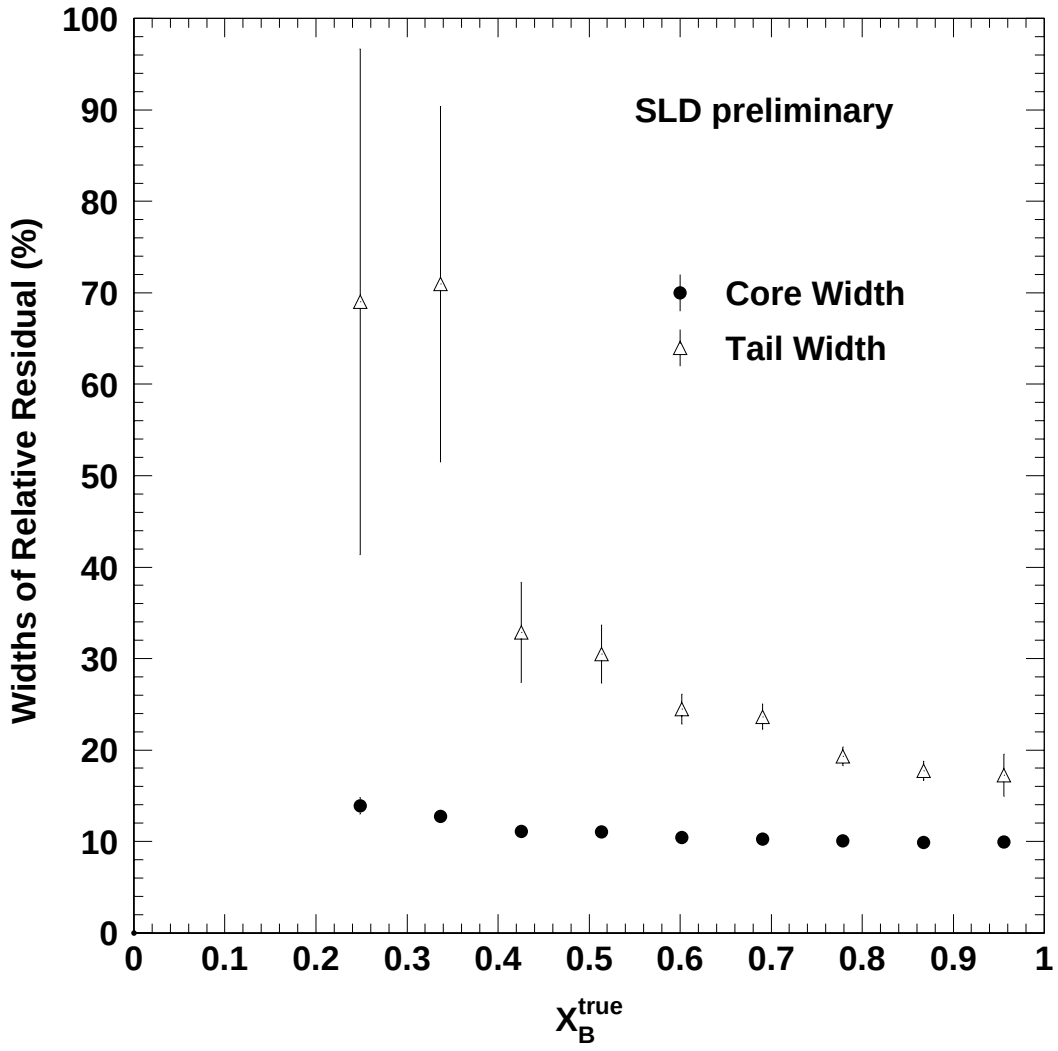

Figure 10: The fitted core and tail widths of the B energy resolution as a function of the true scaled B hadron energy. The ratio of the amplitude of the inner Gaussian (core) to that of the outer Gaussian (tail) is 83:17.

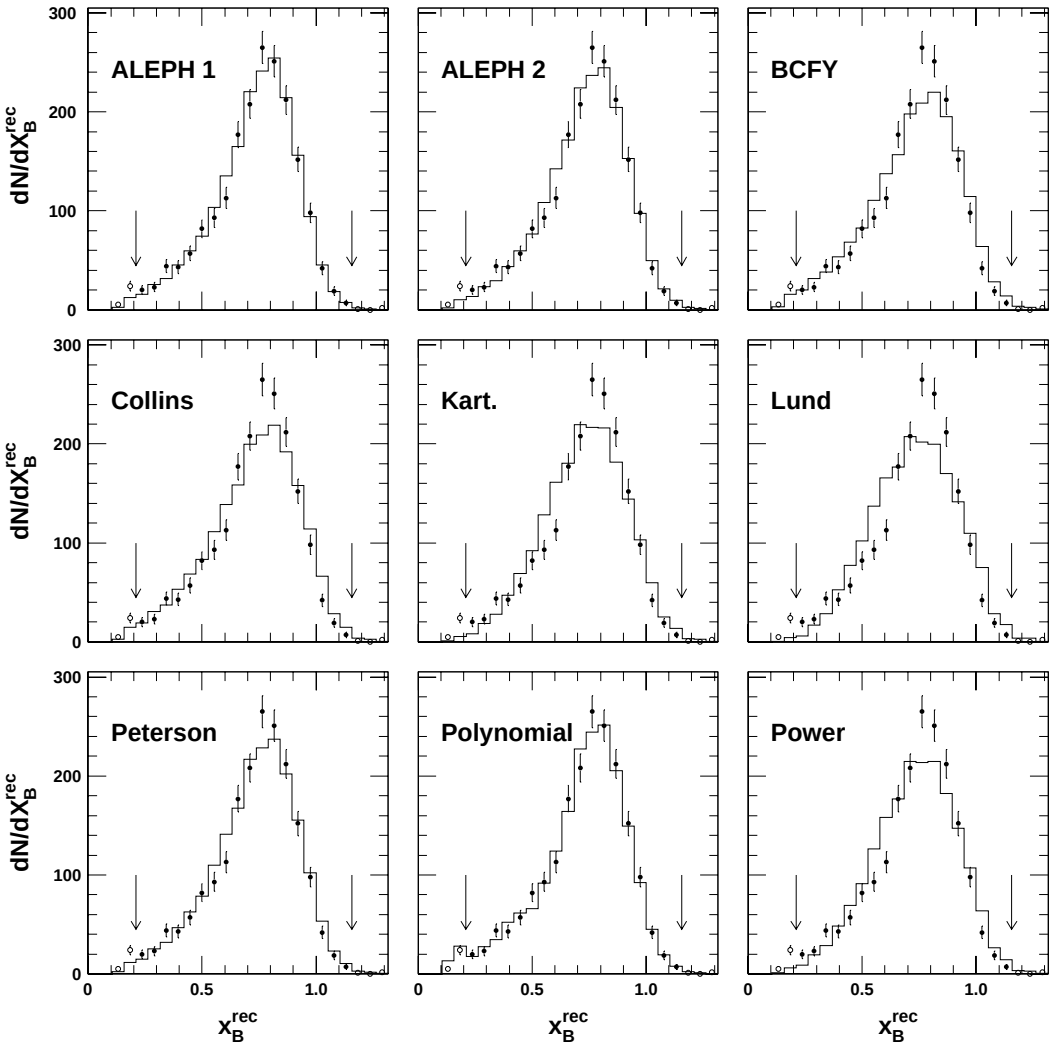

Figure 11: Each figure shows the background-substracted distribution of reconstructed B hadron energy for the data (points) and for the simulation (histograms) based on the respective optimised input fragmentation function. The χ^2 fit uses data in the bins between the two arrows.

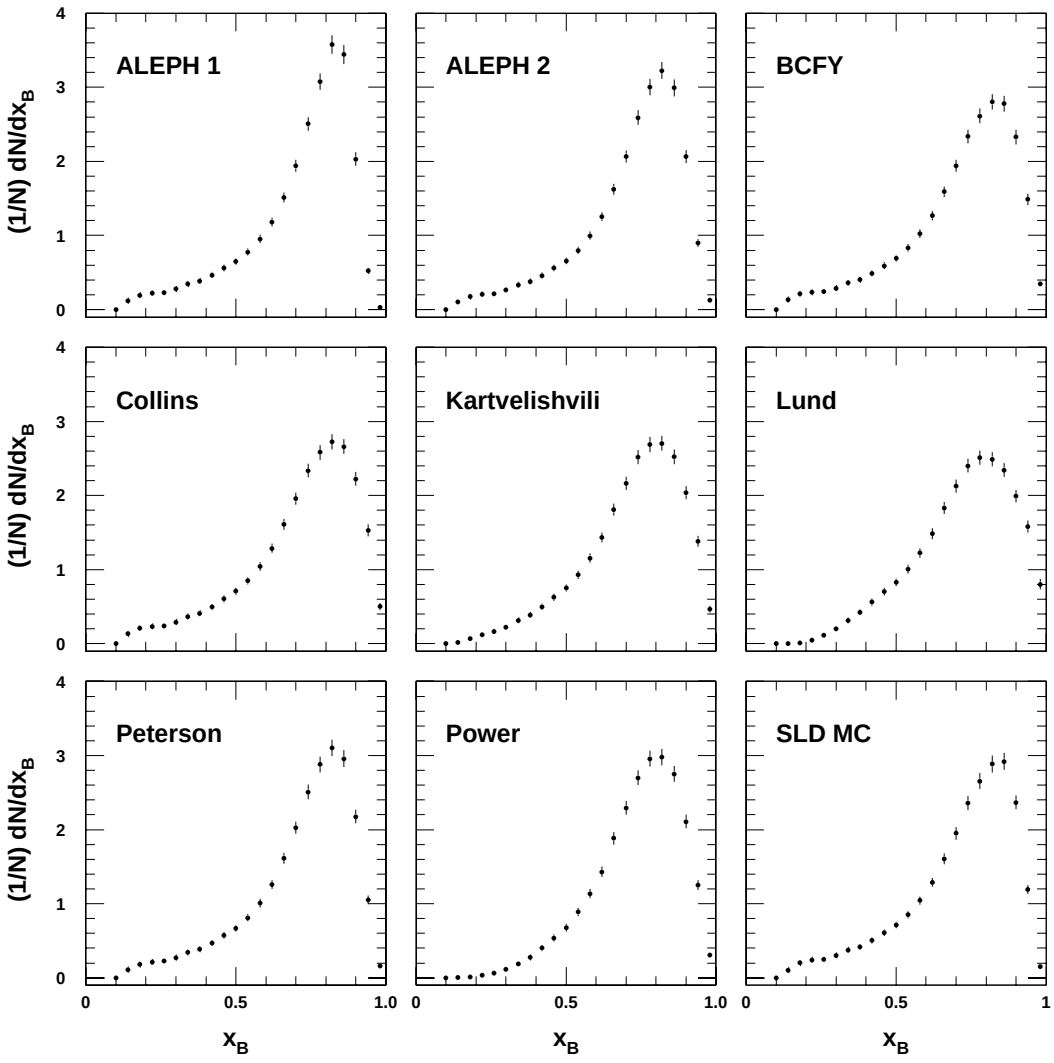

Figure 12: The data distributions of scaled B hadron energy corrected using simulations based on different input B fragmentation functions (see text). Statistical error bars are shown; these are highly correlated between bins and among the sets of results. The bottom-right plot is the unfolded distribution using the default SLD Monte Carlo simulation.

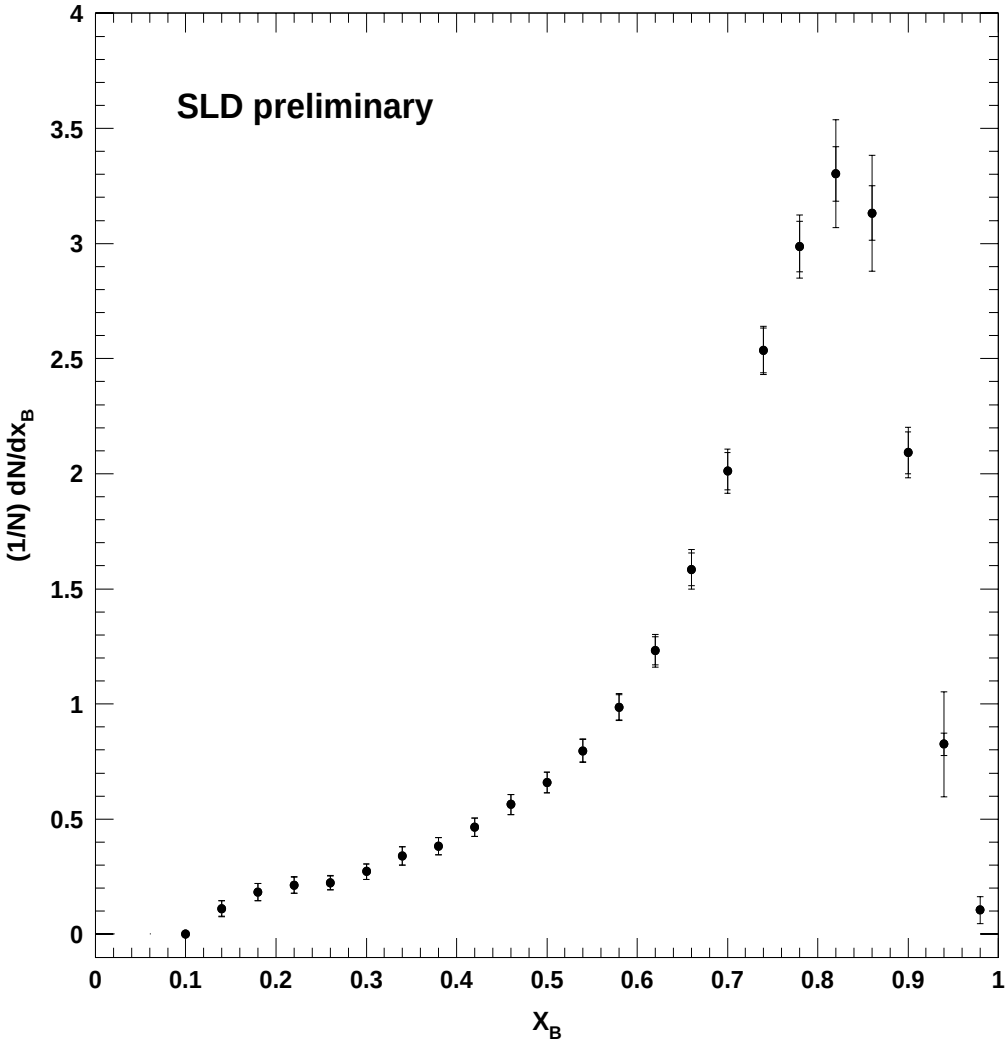

Figure 13: The final corrected distribution of scaled B hadron energies. In each bin the statistical error is indicated by the inner error bar, the quadrature of sum of statistical and unfolding errors by the outer error bar. Systematic errors are not included. Note that the first two bins are below the kinematic limit for x_B (no point shown).